



Basic Neuroscience

A system to measure the Optokinetic and Optomotor response in mice

Friedrich Kretschmer*, Szilard Sajgo, Viola Kretschmer, Tudor C. Badea*

Retinal Circuit Development & Genetics Unit, Neurobiology Neurodegeneration & Repair Laboratory, National Eye Institute, National Institute of Health, Bethesda, MD, USA



HIGHLIGHTS

- A novel system for automated detection of Optomotor and Optokinetic responses under identical stimulation conditions reveals parallels between the two reflexes.
- Novel tracking algorithms allow the accurate representation of complex visually evoked head movements.
- We provide the blueprints for inexpensive hardware, and release open source software for our system, making it easy to replicate.

ARTICLE INFO

Article history:

Received 30 April 2015

Received in revised form 4 August 2015

Accepted 5 August 2015

Available online 14 August 2015

Keywords:

Mouse

Vision

Retina

Behavior

Optomotor response

Head movements

Optokinetic reflex

Eye movements

Video tracking visual field

ABSTRACT

Background: Visually evoked compensatory head movements (Optomotor responses) or eye movements (Optokinetic responses) are extensively used in experimental mouse models for developmental defects, pathological conditions, and testing the efficacy of therapeutic manipulations.

New method: We present an automated system to measure Optomotor and Optokinetic responses under identical stimulation conditions, enabling a direct comparison of the two reflexes. A semi-automated calibration procedure and a commercial eye tracker are used to record angular eye velocity in the restrained animal. Novel video tracking algorithms determine the location of the mouse head in real time and allow repositioning of the stimulus relative to the mouse head.

Results: Optomotor and Optokinetic responses yield comparable results with respect to determining visual acuity in mice. Our new head tracking algorithms enable a far more accurate analysis of head angle determination, and reveal individual head retractions, analogous to saccadic eye movements observed during Optokinetic Nystagmus.

Comparison with existing methods: To our knowledge this is the first apparatus allowing the direct comparison of Optomotor and Optokinetic responses in mice. Our tracking algorithms, which allow an objective determination of head movements are a significant increment over existing systems which rely on subjective human observation. The increased accuracy of the novel algorithms increases the robustness of automated Optomotor response determinations and reveals novel aspects of this reflex.

Conclusions: We provide the blueprints for inexpensive hardware, and release open source software for our system, and describe an accurate and accessible method for Optomotor and Optokinetic response determination in mice.

Published by Elsevier B.V.

1. Introduction

The mouse is the most commonly used mammalian model organism due to its fast reproduction cycle, relatively small size and the vast amount of genetic strategies available for gene manipulations, functional manipulations, pathogenetic and therapeutic

studies. Assays addressing the visual system of mice in basic and clinical research applications employ a variety of anatomic and physiological techniques. However the number of established paradigms for assessing overall visual function of the whole animal are limited. Tests can be broadly classified in (i) learning/discrimination assays, in which reward or penalty cues are used to train animals to discriminate visual stimuli, and (ii) tests addressing discrete visual reflexes, such as circadian photoentrainment, pupil constriction or vestibulo-ocular coordination. The reflex responses do not require training and can be easily quantified resulting in objective measures of visual function. During locomotion, animals integrate vestibular, proprioceptive and visual

* Corresponding authors.

E-mail addresses: friedrich@openetho.com (F. Kretschmer), tudor.badea@nih.gov (T.C. Badea).

URL: <http://openetho.com> (F. Kretschmer).

information to minimize apparent image motion across the retina. Compensatory eye (Optokinetic responses, OKR) or head/body movements (Optomotor responses, OMR) can be elicited when vestibular input is dissociated from visual information, by simulating a global movement of the visual surround. The measurement of these responses is a widely established method to assess various parameters of the visual system in the context of impaired visual function caused by disease models or developmental defects (Prusky et al., 2004; Anstis et al., 1998; Tappeiner et al., 2012). In this study we present a largely automated system to evoke, record and objectively quantify Optokinetic and Optomotor responses in mice.

1.1. Evoking the Optomotor and Optokinetic reflex in mice

To evoke Optokinetic and Optomotor reflexes in mice the animal is typically placed in the center of a cylinder or sphere that is covered with a repetitive pattern, such as stripes (Thaung et al., 2002; Abdeljalil et al., 2005), sinusoidal gratings (Prusky et al., 2004), or random dots (Dubois and Collewijn, 1979). The pattern is rotated around the animal at a constant velocity (Prusky et al., 2004) in one (Prusky et al., 2004; Abdeljalil et al., 2005) or alternating directions (Kretschmer et al., 2013). Alternatively the velocity can be changed sinusoidally (van Alphen et al., 2010; Kretschmer et al., 2012). These patterns can be painted or projected onto the inner surface of card board, plastic or wood cylinders as previously described for OKR or OMR experiments in mice (Thaung et al., 2002; Mitchiner et al., 1976; Mangini et al., 1985; Schmucker et al., 2005) and other species (Easter and Nicola, 1996; Beck et al., 2004), generating a complete 360° image at a homogeneous distance from the animal. Centering in the horizontal plane can be achieved by restraining the animal (Stahl et al., 2000; Mangini et al., 1985; Mitchiner et al., 1976) when measuring OKR. When measuring OMR, the freely moving animal can alter its distance to the walls of the physical cylinder, and therefore the perceived spatial frequency of the objects presented on the wall. Thus the tested spatial frequencies vary during the experiment. Digital presentation techniques (with projectors (Rinner et al., 2005; Kretschmer et al., 2012) or monitors (Prusky et al., 2004; van Alphen et al., 2009; Benkner et al., 2013; Kretschmer et al., 2013)) significantly speed up experiments by allowing the presentation of a large array of stimuli in quick succession. By simulating a virtual cylinder a constant grating can be presented in the field of view of the animal. The actual physical distance to the stimulus has to be readjusted dynamically based on the location of the animal, either manually, by the observer (Prusky et al., 2004), or automatically through software control (Benkner et al., 2013; Kretschmer et al., 2013).

Perspective errors in the vertical dimension, as perceived at the top or bottom ends of the cylinder are not accounted for in case of the OMR but can be compensated by using a virtual sphere during OKR measurements (van Alphen et al., 2010).

1.2. The measurement of the Optomotor response in mice

During OMR measurements, stimuli consisting of striped patterns with distinct luminosities, contrasts, spatial or temporal frequencies can be presented in a sequential (Schmucker et al., 2005; Kretschmer et al., 2013) or step-wise manner (Prusky et al., 2004; Umino et al., 2008; Benkner et al., 2013). The ability of mice to detect and react to these stimuli by head/body movements is judged for each individual condition by a human observer (Prusky et al., 2004; Umino et al., 2008) resulting in determination of threshold criteria (Thaung et al., 2002; Prusky et al., 2004). Typically these experiments are performed using a two-alternative, forced-choice protocol. The observer has to decide whether the mouse performed OMR (Prusky et al., 2004) or has to determine the direction in which

OMR occurred (Umino et al., 2008). The determined visual acuity thresholds therefore depend on the subjective judgment and experience of the observer, resulting in an error-prone and time intensive procedure. Thus, automatic head/body detection is desirable. Body movements in mice were previously quantified using video-tracking by determining the speed of movement of the center of mass and the angular body velocity derived through a linear regression of the whole body (Schmucker et al., 2005). A different approach used an automated approximation of the head movement (based on the snout location and the center of mass) to determine whether or not an animal saw a stimulus (Benkner et al., 2013). Based on this binary “yes” or “no” decision the spatial tuning of the visual system was derived by determining a contrast sensitivity curve. We previously presented a method for automatic head movement measurement during OMR experiments (Kretschmer et al., 2013). By computing the fraction of time tracked during 1 minute, spatial frequency dependency curves can be derived directly from the recorded angular head movements. The actual velocity of the head during OMR has never been analyzed in mice. The existing methodologies quantify all stimulus correlated behavior within a certain velocity range. This range inherently depends on the quality of the video tracking algorithm and does not necessarily rely on the actual velocity of the body or head during OMR. A linear regression through the thresholded pixel area of the mouse body was used to determine the body axis in Schmucker et al. (2005). The authors used a velocity threshold of $\leq 50^{\circ}/s$ to discard methodological artifacts. A different study (Benkner et al., 2013) used commercial tracking software (Viewer3, Biobserve GmbH, Germany) and approximated the head location based on the snout location and the center of mass. The authors used a velocity threshold of $\leq 2.5 \times$ stimulus velocity to discard irregular movements. In another previous study (Kretschmer et al., 2013) tracking behavior was defined as head movements in the correct direction at an angular velocity of less than $9^{\circ}/s$ ($0.8 \times$ stimulus velocity at $12^{\circ}/s$). Thus, existing video-tracking algorithms overcome the subjectivity of approaches based on human observers, however are limited by reduced accuracy and low signal to noise ratios. In addition, a clear quantification of actual head angle and velocity, are not possible.

1.3. The measurement of the Optokinetic reflex in mice

Visual function in mice can also be analyzed using OKR measurements, in which the head of the mouse is restrained, and the eye position is determined using either magnetic coils or video tracking of pupil position. Since the eye has to stay in focus throughout such recordings the measurement typically requires a restraint of the animal. While the animal can be restrained in a non-invasive way using a restrainer box (Mitchiner et al., 1976; Sinex et al., 1979) the quality of the recordings is not good enough to quantify responses in an automated way and derive measures like the gain from the data. Instead these studies rely on human observation. A much better signal to noise ratio can be achieved by fixing the animal by gluing (Iwashita et al., 2001; Sakatani and Isa, 2004) or screwing (Stahl et al., 2000; Cahill and Nathans, 2008) a holder to its skull.

When measuring OKR the performance of an animal's visual system is traditionally assessed by quantifying the gain of the eye movement (Stahl et al., 2000; van Alphen et al., 2009). The velocity at which the eye follows and the derived gain are parameters which can only be calculated by estimating the rotation center of the pupil. This data can either be approximated by assuming a general eye model (Iwashita et al., 2001) or it can be derived for each individual animal by calibrating the system (Stahl et al., 2000). The calibration procedure is performed to estimate the angle the eye moved based on the pixel coordinates determined by the eye tracker. This task is more difficult in rodents, since they are avofeate and cannot be asked or trained to focus on a defined point in space. To circumvent

this limitation, typically several images of the eye are taken from various angles. The distance of the pupil from the center of corneal curvature is indirectly derived from these images based on the pixel distance of the pupil to one or more corneal reflections generated by a stationary light source (Stahl et al., 2000). This procedure is time demanding and requires precise control of the position of the camera to set it to a specific rotation and distance from the animal. Thus OKR determinations are an accurate, but more demanding approach compared to OMR analysis.

1.4. Motivation

Measurements of OMR in mice are far more common than measurements of the OKR. Beside the fact that these measurements are non-invasive and do not require a complicated calibration procedure, the most important reason might be the commercial availability of a device to measure OMR (*Optomotry* by CerebralMechanics Inc.). While the OMR serves as a common and useful tool to measure parameters of the visual system, the actual reflex, i.e. the movement of the mouse head in response to large scale visual stimuli, was never systematically analyzed in mice. A reason for this might be the lack of a suitable video tracking algorithm to determine the head and body angle precisely enough during an experiment. Commercially available tracking algorithms typically determine the center of gravity of the animal and the location of the snout and tail. These coordinates can only give a rough estimate of the head angle. For example it can be calculated as the difference between the angle of the vector from the tail to the snout and the angle of the vector from the center of gravity to the snout. This estimate is sufficient to determine whether OMR was induced or not (Benkner et al., 2013), but is not precise enough for a quantitative analysis of the occurring head movements.

Given the technical peculiarities of the two reflexes, it is unclear how the OMR and OKR relate to each other and it is hard to directly compare threshold parameters determined through either methodologies because of the varying stimulus conditions and different setups that were used in previous publications. Beside the direct comparison of these two reflexes, our main goal was to develop a system that combines the advantages of previously published methodologies to measure OMR and OKR sequentially to enable routine measurements of both reflexes in mice for the study of disease models, developmental defects, genetic manipulations and drug treatments using the highest possible degree of automation.

2. Materials and methods

2.1. Hardware

We have built a setup to evoke Optokinetic and Optomotor responses in mice. All components are mounted inside a custom built box 652 mm × 652 mm × 404 mm build from 30 mm × 30 mm extruded aluminum profiles (Bosch Rexroth, Germany). The box was designed using FreeCAD (the design files and all other software components can be downloaded from <http://openetho.com/download/> or obtained by email from the corresponding authors.). The box accommodates four 23 in. LCD screens that surround the animal. The setup can quickly be reconfigured to measure either the Optomotor responses or the Optokinetic reflex.

2.1.1. Stimulus presentation

Stimuli are presented on four computer screens surrounding the animal covering the whole field of view with a texture projected onto the surface of a virtual sphere (see Fig. 1c). The sphere is positioned in such a way that the animal is always located at its

center. Hence the distance to all areas of the stimulus is held constant. OpenGL was used for the perspective projection of the sphere. Additionally a sphere with a radius one pixel smaller than the main sphere is rendered inside the larger sphere. This secondary sphere is transparent by default but can be covered with a solid or semitransparent texture to mask parts of the stimulus. Both spheres can be independently rotated about arbitrary axes and hence can be used to present any kind of horizontal, vertical or diagonal movement. The radius of the virtual sphere was set to 288 mm – this corresponds to $\approx 0.55 \times$ the width of the computer screens. This radius minimizes the difference between the real distance of the animal to the screens and the virtual distance of the sphere (Kretschmer, 2012). The software can also be used to present a virtual cylinder instead of a sphere.

We used four S23A700A 23-Inch (Samsung, South Korea) screens for stimulation. These screens were chosen because of their small panel frame border. The panels 120 Hz LCD module is illuminated by an LED back light that produces relatively little heat. The panels (523 mm × 302 mm) were removed from their plastic casing and were slid into plastic rails on each side of the box. The heat sinks on the back of the panel circuit boards touch the outer aluminum plates to passively transfer the heat to the outside. An EAH6950 graphic card (ASUSTeK Computer Inc., Taiwan) was used to drive the four screens that were connected through DisplayPort DVI-D Dual-Link Adapters (Accell B087B-002B). A fifth screen, placed outside the box, is used to display the image recorded by the camera and the graphic user interface and control the experiment. It was connected to the internal graphics card (ATI Radeon HD 4250) on the Motherboard trough DVI. Additional acrylic anti-glare sheets (TAP Plastics, CA, USA) were placed in front of each panel leaving a small space in between to accommodate neutral density filters. These acrylic sheets also simplify cleaning of the arena. To reduce the luminosity levels of the LCD screens to scotopic light conditions we used gel sheet 211.9 neutral density filters (Lee Filters, UK), cut to size and placed in Polyester Film sleeves (TAP Plastics, CA, USA) in front of the screens. Each filter reduces the light intensity by ≈ 1 log unit (transmittance: 12.5%). By stacking two filters, the light intensity can be reduced by ≈ 2 log units. The three color channels of the four screens result in a combined light intensity of 9×10^{10} Qs/cm². This intensity was measured at the center of the platform using a 0.2 cyc/^o grating. The Michelson contrast ($C_M = (L_{max} - L_{min})/(L_{max} + L_{min})$, for the maximum and minimum luminances) of the gratings was 100% (at the maximum color values).

A PC was used to drive the stimulation and perform the head tracking. We used a system with a AMD FX-8150 CPU running on a M5A88-V EVO AM3+ board (ASUSTeK Computer Inc., Taiwan), with 8 GB of RAM. A 128 GB SSD (510 series, Intel, CA, USA) was used during an experiments for recordings. An additional 2TB HDD (Deskstar 5K3000, Hitachi, Japan) was used to store the data.

Measurement of the Optomotor response. In the OMR measurement configuration (Fig. 1a) the bottom of the box is covered with a mirror (532 mm × 532 mm) with a 50.8 mm hole in its center. It is held in place by plastic rails which allow us to quickly remove it for cleaning.

A round platform (50.8 mm) is positioned in the center of the arena (at a distance of ≈ 262 mm using a short vertical aluminum profile (184 mm) attached to a horizontal profile running below the mirror. A second mirror (same size as the bottom mirror) is mounted to the top lid. The mirror is held in place by light-tight 8 mm glazing strips. The lid itself is mounted to the box through sliding door guides. Its edges are covered with rubber seals to allow a light-tight closure. All small parts were acquired from the Bosch aluminum framing catalog (Bosch Rexroth, Germany). A Pro 9000 camera (Logitech, Switzerland) is mounted at the center of the top lid to record head movements and is connected to the main PC

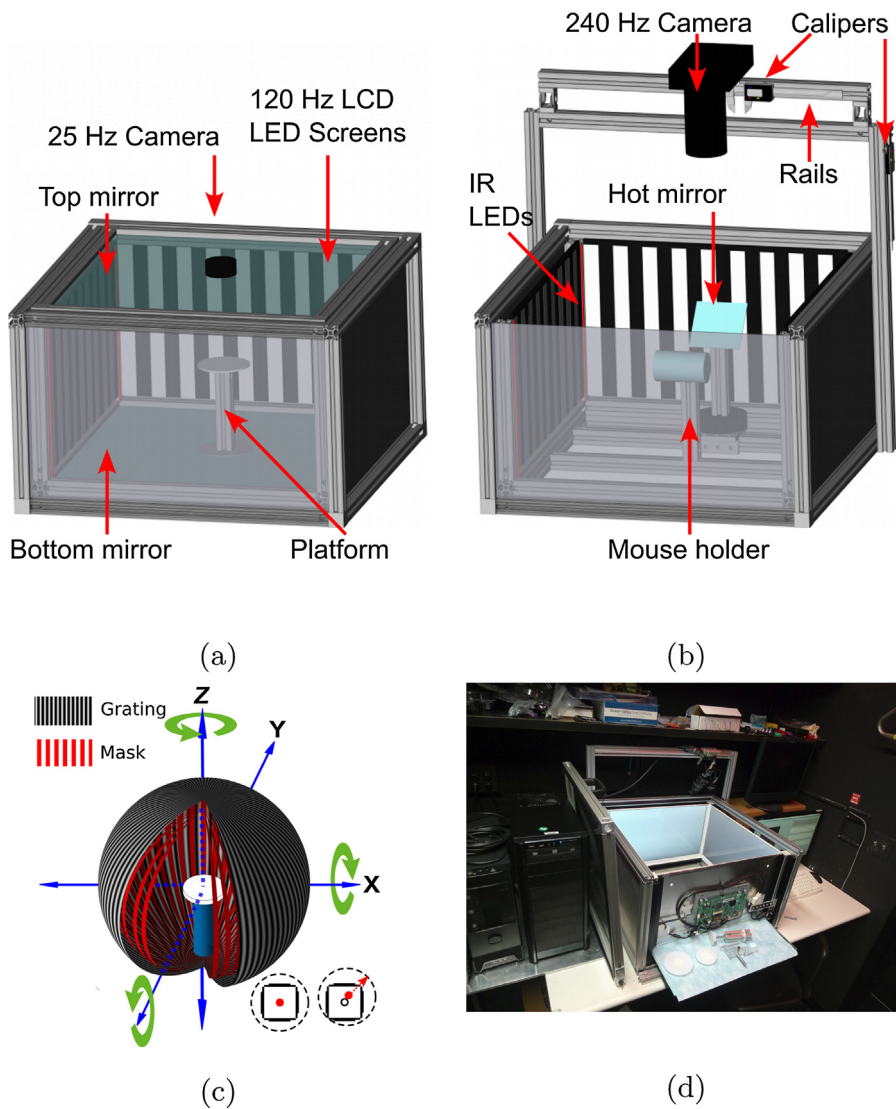


Fig. 1. The setup can easily be converted between condition (a) to measure the OMR in the freely behaving animal and condition (b) to measure OKR in the head fixed animal. In both cases the animal is located inside a virtual sphere (c) that is presented on the four computer screens surrounding the animal. This sphere is adjusted in such a way that the animal is always located in its center (inset in (c)). (d) The lid, mirror and platforms can easily be removed.

through USB. The PCB of the camera was removed from its casing and was directly screwed onto an acrylic sheet, which was attached to the mirror.

Measurement of the Optokinetic response. For OKR measurements an acrylic holder replaces the platform (see Fig. 1). The animal is fixed to this holder by its head implant. A hot mirror is located next to the animal's eye to observe the eye from above under infrared illumination using an ETL-200 (ISCAN, Burlington, MA, USA) video camera. The hot mirror appears transparent to the animal and hence the stimulus can be presented in the entire field of view. The hot mirror is mounted on a 70 mm rotary stage (Edmund optics, NJ, USA) to allow a precise adjustment of the angle, required for the calibration of the system (see Section 2.2.2). The camera can be translated smoothly in either the horizontal plane or vertical plane (for focal adjustments) using sliding carriages (OpenBuilds Part Store, NJ, USA) mounted on rails. Two electronic calipers (LCD Digital Vernier caliper 150 mm, CE Compass, CA, USA) were attached to the horizontal rail and one of the vertical side beams, allowing precise determination of the camera position (see Section 2.2.2). We used the DQW Acquisition software (ISCAN, Burlington, MA, USA) to record the pixel coordinates of the pupil and reflection. The recording was triggered remotely by the *okr arena* software

module through RS-232. The recorded data was transferred automatically to the main PC through the same interface after each trial and stored on the hard drive.

2.1.2. Infrared light conditions

In order to record under infrared light conditions we removed the infrared cut-off filter from the camera by unmounting the circuit board from its original casing, and used an injection needle to break out the glass filter. The infrared filter is located inside the autofocus unit, which has to be unsoldered in order to access the filter on this model. We determined the thickness of the filter under a microscope (300 µm) and glued two 150 µm coverslips at its original position in order to maintain the auto-focus function. The circuit board was then screwed on to a polyethylene sheet which was centered and glued into the hole of the top mirror. We added 950 nm IR strips (Elemental LED, CA, USA) in all four edges of the arena to provide general illumination (see Fig. 2a). The led strips were connected in series and their intensity/voltage could be controlled through an external DC power supply (R.S.R. Electronics Inc., NJ, USA) that allows us to alter the level of general illumination. To keep the lighting conditions as constant as possible under all stimulus conditions, an additional 25 mm infrared bandpass filter was

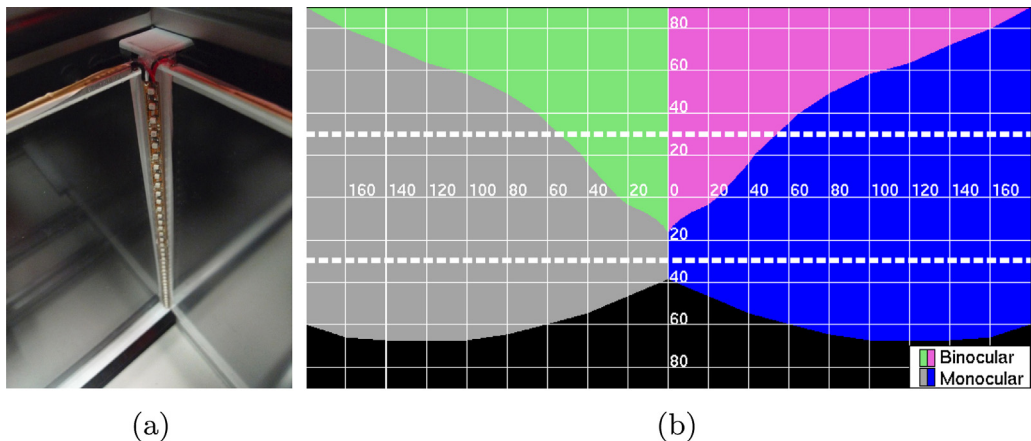


Fig. 2. (a) Infrared illumination is provided by infrared LED strips attached in all four edges inside the setup. (b) Masks to cover the left binocular field (green), right binocular field (magenta), left monocular field (gray) and right monocular field (blue). The dashed lines represent the visual field that is covered by the four screens. Areas based on Dräger (1978).

added in front of the camera (RT-830, Edmund optics, NJ, USA) to balance the luminance.

2.2. Software

The software consists of several interconnected modules. A main program written in MATLAB (The MathWorks Inc., MA, USA) connects the various components (Fig. 3) and provides a centralized graphical user interface to monitor and control experiments (Fig. 4). In brief, stimuli are generated by the *patterGen* module. These stimuli are used by *okrarena* to render the virtual sphere. Head tracking is performed by the *omr monitor* module. The commercial ETL200 system is used for eye tracking and communicates with the MATLAB program.

Stimulus generation. Stimuli were designed using a custom MATLAB program *patterGen*, an improved version of the program described in Kretschmer et al. (2013). This program is used to generate gratings, masks and rotation protocols. **Gratings** are mapped as textures on to the virtual sphere. We implemented routines to generate random dot patterns, saw-tooth, sinusoidal or square-wave gratings at arbitrary spatial frequencies. All patterns are initially generated as grayscale images. In a second step these pattern can be “colorized” to set a specific contrast or color schema. To allow a linear color and contrast adjustment all color values are color corrected based on the opto-electrical transfer function of the LCD panels we used. For this purpose we measured the luminance at various intensities for the three color channels of the screens using a calibrated spectrometer (USB-4000, Oceanoptics, Inc., Dunedin, FL, USA). All patterns are internally stored as PNG files. In case of vertical gratings the patterns are stored as one individual line of pixels, in case of horizontal gratings as one pixel column. This significantly reduces space and loading time of these patterns. Additionally, pattern **masks** can be generated from within the program to cover parts of the visual field of the animal. We implemented various generators for the masks. The mask can be used to obscure steradians of arbitrary sizes within the field of view of the animal. Based on previous literature (Dräger, 1978) we also designed masks specific for the visual field of the mouse that cover only the monocular or binocular field of one or both eyes (see Fig. 2). Masks are also stored as PNG files. Transparency is realized through the alpha channel this format offers.

The rotation of the stimulus was realized through **rotation protocols**. These protocols contain a series of values for each refresh of the LCD monitors that describe the rotation of the sphere. Internally

these protocols are stored as text files containing comma separated values, as required for the use with *okrarena*. We implemented rotations at arbitrary velocities and amplitudes as well as rotations at sinusoidally changing velocities (pendular movements).

A combination of a grating, a mask and a rotation protocol can be added to a list. A list contains a sequence of stimuli that can be presented consecutively during an experiment without human interaction. The order of the stimuli within a list can be randomized.

Stimulus presentation. The stimulation on the four screens was realized through an improved version of the standalone program *okrarena* (Kretschmer et al., 2013, GPLv3, freely downloadable at openetho.com) which uses OpenGL and the Simple DirectMedia Layer. We used this program to render the main sphere and the masking sphere on the four screens. *okrarena* can remotely be controlled through TCP/IP. In the described setup all programs (except for the eye tracking software) were running on the same PC and communication hence only occurred on a local socket. TCP/IP was realized from within MATLAB using JTCP (Kevin Bartlett, MATLAB Central). Once a set of stimuli is created (see Section 2.2) and the experiment is started, the main MATLAB routine calls the separate program *okrarena* that receives all previously generated files as startup parameters. The MATLAB program then connects to *okrarena* to update the cylinder position based on the position of the animals head determined by the head tracking module (see Section 2.2.1).

2.2.1. Head movements

Head movements are recorded by the top camera in the lid. We track the animal's head movements during an experiment and use the calculated head angle to automatically quantify the Optomotor response for each stimulus condition.

Head tracking algorithm. Two tracking algorithms were used to determine the location of the head:

A slightly modified version of the previously described algorithm (Kretschmer et al., 2013) was used during the experiment to determine head position. This location is used to translate the virtual cylinder to keep the distance to the cylinder wall constant.

A novel tracking algorithm was used offline, after the experiments, to accurately determine the head angle and quantify tracking. The previously published version performs reliably under bright illumination (Kretschmer et al., 2013), however it is less effective for some coat colors, under infrared illumination and/or dim light conditions.

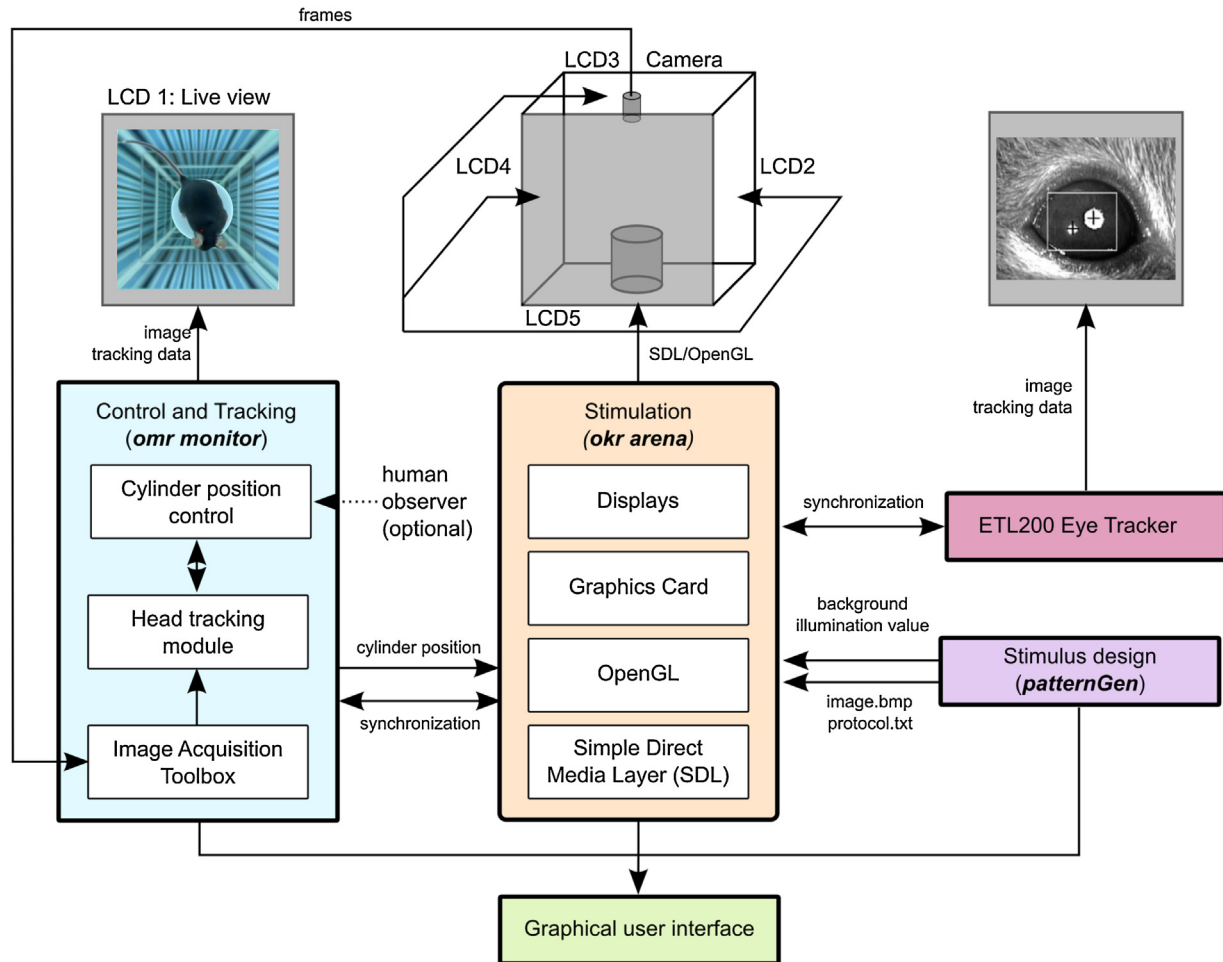


Fig. 3. Software architecture of the system. The stimulus is presented on four screens by the program *okr arena*. This program receives images that are used as textures on the virtual sphere and protocols that describe the rotation of the sphere. These files were previously generated through the MATLAB routine *patternGen*. Head movements (OMR) are recorded with a camera at 25 Hz, which feeds the program *omr monitor*. This program records the video and determines the animal's head position. The head position is stored and communicated back to *okr arena*, which readjusts the position of the virtual sphere accordingly. To record eye movements (OKR) the ETL200 Eye tracker is remotely triggered by the stimulation software. The location of the pupil and cornea are read out at 120 Hz and are continuously buffered for storage. The experiment is controlled with a centralized graphical user interface.

The new version overcomes these issues, yields a better signal to noise ratio and runs much faster. It can compute real time data at up to 50 fps on an AMD FX-8150 CPU and thus is fast enough to be used for online visual stimulus repositioning. The algorithm currently runs within a standalone executable program and was implemented in C using the Open Source Computer Vision library (OpenCV, Willowgarage/Intel). The novel approach uses the contours in the image as a basis for all computation. It consists of: (a) image thresholding, (b) mouse contour determination, (c) identification of the snout position, and (d) determination of the head angle.

(a) A range threshold is applied on all three color channels to segment the image.

The color values of the image $I = (i_{k,l}) \in \mathbb{R}^{w \times h}$ with the height h and the width w are $i_{k,l} \in [0, 255]$ for all k, l . With the help of two threshold values $s_1, s_2 \in [0, 255]$ a binarized image $BI = (bi_{k,l}) \in \{0, 1\}^{w \times h}$ can be calculated:

$$bi_{k,l} = \begin{cases} 0, & \text{if } i_{k,l} \leq s_1 \vee i_{k,l} \geq s_2, \\ 1, & \text{if } s_1 \leq i_{k,l} \leq s_2. \end{cases} \quad (1)$$

(b) The contour and the areas of all binary objects are derived from the binary image through the *FindContours* function of OpenCV (Suzuki et al., 1985). Instead of using the largest object within a region of interest (Kretschmer et al., 2013) we introduced

more specific geometric constraints that are applied consecutively (see Fig. 5e) to discriminate the mouse shape from other contours:

1. Contours outside of a certain area range ($10,000 \text{ px} \leq \text{area} \leq 40,000 \text{ px}$) are discarded.
2. Contours that do not cross at least three of the four quarters of the image (e.g. animals snout in upper left part of image, the hind part of the body in the bottom right and bottom left part of the image) are discarded.
3. The contour of the animal is then defined as the contour with the closest center of mass to the center of the image.

Based on this contour \mathcal{M}_t , defined as the set of pixel positions M_t , at time point t we calculate the reference locations on the body. The hindquarters are calculated as the center of gravity, which lies toward the back of the animal. The center of gravity Cog_t of the set \mathcal{M}_t at timepoint t is calculated as:

$$Cog_t = \frac{1}{|\mathcal{M}_t|} \sum_{M_t \in \mathcal{M}_t} M_t, \text{ with } |\mathcal{M}_t| \text{ the number of elements} \quad (2)$$

The point $C_t \in \mathcal{M}_t$ farthest away from the body center Cog_t is used to determine the rough location of the head:

$$C_t \in \arg \max_{M_t \in \mathcal{M}_t} \|M_t - Cog_t\| \quad (3)$$

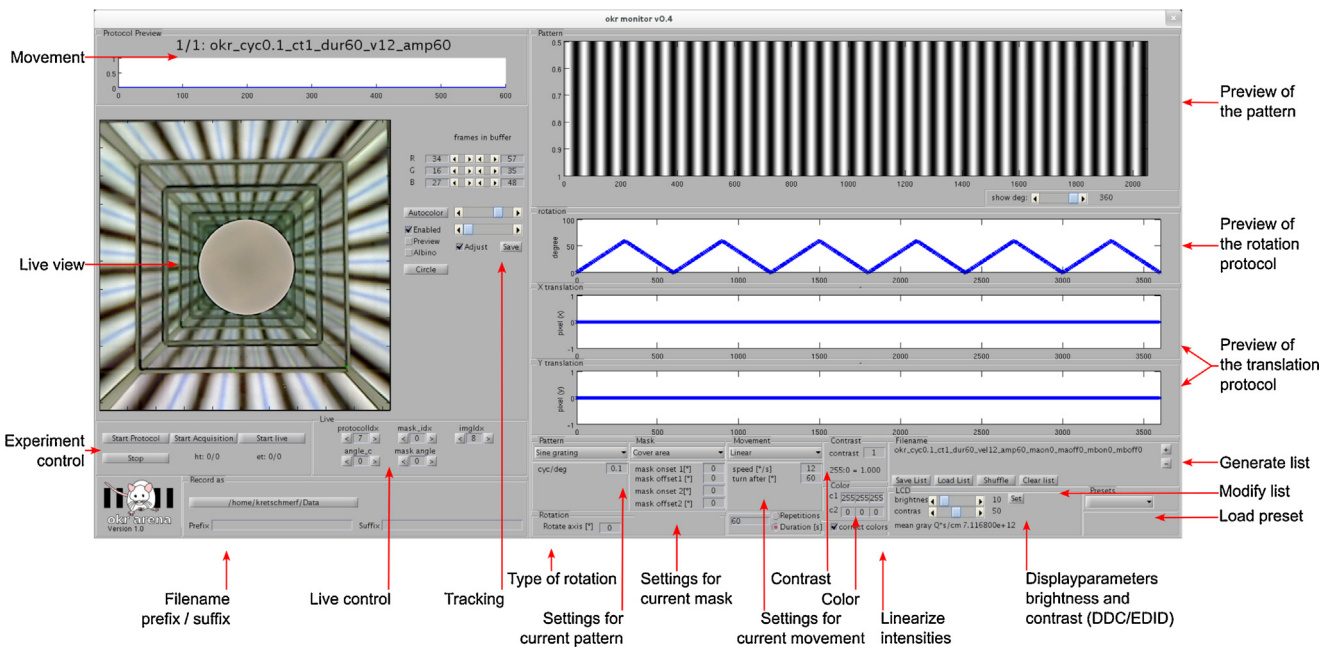


Fig. 4. The graphical user interface. New stimuli can be generated in the right panel of the window. A stimulus consists of an image that is used as a texture on the virtual sphere, a mask that can cover areas of the sphere and a protocol that describes the movement of the sphere and the mask over time. Stimuli can be added to a list, which can then be run without human interaction. The left panel shows a live view of the inside of the arena with the platform and a set of user interface elements to set the parameters of the tracking algorithm. This is also where the user can set the recording path and start and stop an experiment.

(c) Snout identification (Fig. 5): We introduce a novel feature which we named “snout stabilization” that specifically addresses two particular cases, which impaired the quality of tracking in a previous implementation (Kretschmer et al., 2013). In some circumstances, the center of mass of the animal does not lie in its hind quarter but is located more frontally. This happens often with very thin animals or animals that stretch their body during the experiment. Hence the detection of the snout fails and the tail is detected instead. Additionally, throughout all recordings animals tend to rotate their head along the long axis of the head (roll rotation) or the interaural axis (pitch rotation) resulting in only a very small area of the snout being visible (or not visible at all). In these situations the snout is mistakenly detected on either the right or the left part of the head, e.g. at the insertion of the ear lobe into the head (compare Fig. 5c with 5f). Both issues not only reduced the quality of tracking but led to the necessity of manually going through all recordings to exclude such periods. These issues can be solved for tracking periods during which pitch and roll axes are relatively constant by the following procedure. The algorithm remembers the locations of the head from the previous frame and rotates the calculated center of mass from the current frame around the snout location of the previous frame in increments of 1° , to minimize the Euclidean distance between the previous head location and the current head location (see Fig. 5f). In practice the center of gravity is rotated in a range of -30° to $+30^\circ$ from its original position around the snout location from the previous frame. For each iteration the algorithm calculates the point farthest away from each rotated center of gravity. The one closest to the location of the previous frame is picked as the new snout location.

Hence we rotate the center of gravity Cog_t around the point C_{t-1} (from Eq. (3)) of the previous frame recorded at $t-1$ by the angle θ by a 2D rotation:

With (x, y) , the coordinates of Cog_t and $(x_{C_{t-1}}, y_{C_{t-1}})$ the coordinates of the snout in the last frame, the rotated coordinates (x', y') can be calculated as:

$$x' = \cos(\theta) \cdot (x - x_{C_{t-1}}) - \sin(\theta) \cdot (y - y_{C_{t-1}}) + x_{C_{t-1}} \quad (4)$$

$$y' = \sin(\theta) \cdot (x - x_{C_{t-1}}) + \cos(\theta) \cdot (y - y_{C_{t-1}}) + y_{C_{t-1}} \quad (5)$$

We perform this operation in a range from -30° to $+30^\circ$ and create a set \mathcal{A}_t of rotated center of gravities Cog'_t . We then calculate the points of \mathcal{M}_t farthest away from each of the rotated center of gravities.

$$\forall Cog'_t \in \mathcal{A}_t \exists C'_t \in \arg \max_{M_t \in \mathcal{M}_t} \|M_t - Cog'_t\| \quad (6)$$

For the new set \mathcal{C}_t of all determined snout locations C'_t we determine the point closest to C_{t-1} by calculating the Euclidean distance between C'_t and C_{t-1} , which defines the new snout location C'_t .

$$C''_t \in \arg \max_{C'_t \in \mathcal{C}_t} \|C'_t - C_{t-1}\| \quad (7)$$

(d) Head orientation: (see Fig. 5) Typically, there is a fair amount of pixel noise occurring right at the edge of the shape. This noise is especially pronounced in the snout region due to the whiskers and the inhomogeneous color caused by the interrupted fur coverage in this area. These considerations make the direct use of the snout position as a reference point for head angle determination impractical. We therefore determine the head orientation using two additional reference points. (see Fig. 5f), which more robustly define the head orientation. These points are defined as follows.

1. The retrieved snout location derived in (c) serves as the center for two circular regions of interest, the diameter of which should be equal or smaller than the length of the mouse head. The value of both radii r_1 and r_2 is set empirically so that the two locations reflect the anatomy and size of the measured animal.
2. These two radii r_1 and r_2 are used to define two additional contours (cyan and yellow outlines in Fig. 5a-d). The sets corresponding to pixel of the mouse head within the two regions are then:

$$U_{C,r_1} = \{M_t \in \mathcal{M}_t | \|M_t - C''_t\| < r_1\}. \quad (8)$$

$$U_{C,r_2} = \{M_t \in \mathcal{M}_t | \|M_t - C''_t\| < r_2\}. \quad (9)$$

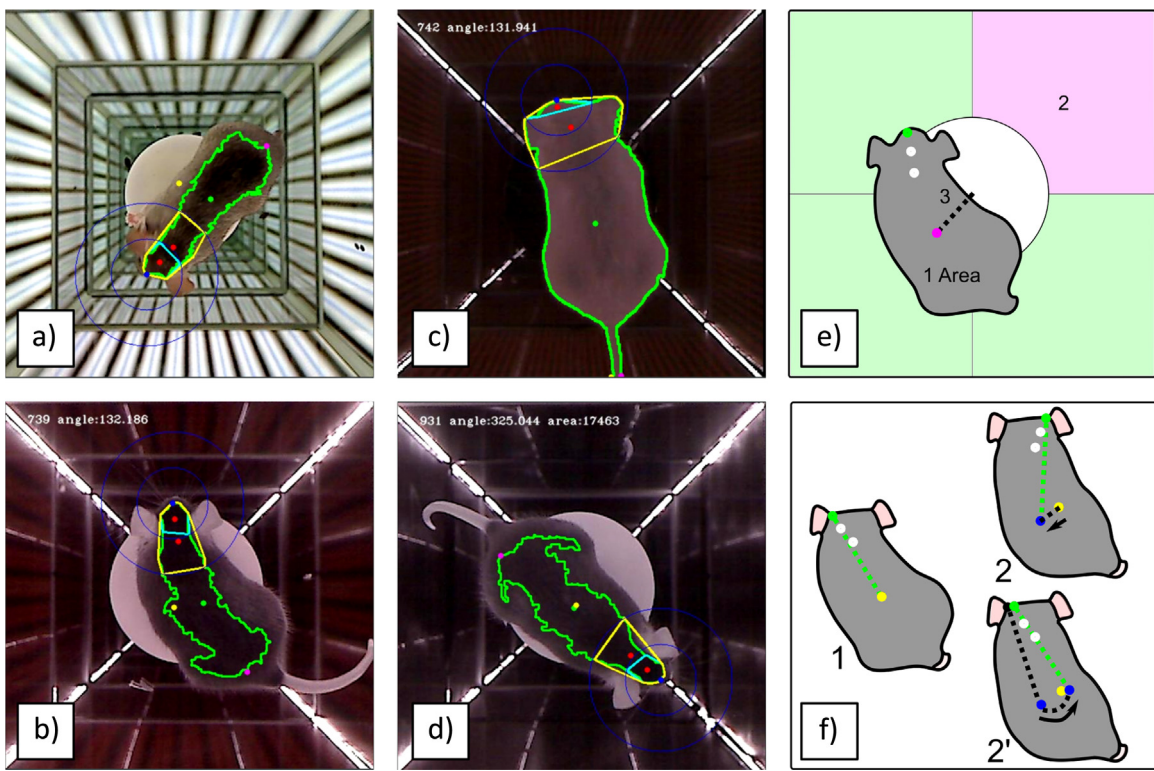


Fig. 5. The new tracking algorithm allows us to determine the head orientation of animals of different coat color under various lighting conditions. To keep the lighting conditions more constant under all stimulus conditions regardless of stimulus type, an additional 25 mm infrared bandpass filter can be placed in front of the camera. (a) A mouse with agouti coat color at photopic light condition without the additional infrared filter. (b) A black coated animal at photopic light condition with infrared filter. (c) An albino animal at scotopic light condition with infrared filter. (d) A black coated animal at scotopic light condition with infrared filter. Colors in a-d: Green line: detected contour of the mouse, green dot: center of gravity, yellow dot: corrected center of mass, magenta dot: "tail" location, blue dot: "snout" location, blue circles: two radii around the snout location, cyan and yellow: the contour within the two radii, red dots: the two points that determine the head location (e) Geometrical constraints to reliably separate the contour of the mouse from the background: 1. The detected contour needs to be within area limits. 2. The contour needs to cross three or more quadrants of the image (green area). 3. The contour needs to be the closest contour to the center of the image. (f) Illustration of the "snout stabilization" method. The snout (green dot) is detected as the point farthest away from the center of gravity (yellow dot). 2. Incorrect snout detection: when the mouse changes its posture the center of gravity shifts (blue) and a different location is detected as the snout (green dot) since it is further from the center of mass (new green segment) In the example the location jumps to the other side of the head. 2', Corrected snout detection method: We rotate the center of gravity (blue dots) around the snout location from the frame 1 (black dot). The point farthest away from this rotated center of gravity lies on the same side as the location determined in 1 (green dot).

3. For each of the contours, two additional centers of gravity Cog_{r1} of U_{Cr1} and Cog_{r2} of U_{Cr2} are calculated. The center of gravity within the first, smaller radius corresponds to a point on the bridge of the snout. The second center of gravity within the larger radius determines the point of rotation of the head. Due to the symmetry of the head these locations are located on the sagittal plane of the head.
4. The head-orientation \vec{g} can be computed as the vector between the two centers of gravity.

$$\vec{g} = Cog_{r1} - Cog_{r2}. \quad (10)$$

A requirement is, that the locations of the head are reliably detected in the first frame that is recorded. This is usually the case since the mouse calmly rests on the platform at this time. If the tail is detected instead of the snout the user can correct this by clicking on the tail with the mouse cursor once only at the beginning of the recording.

Based on these additional refinements the tracking algorithm performs robustly on animals of all ages, sizes and coat colors (including albinos) under all light conditions investigated (Fig. 5).

Determining the optimal dual threshold criterion. There is little information on the ability of mice to match the visual stimulus velocity with their head movements (OMR head gain). During typical recording sessions, mice can occasionally be engaged in

exploratory movements, sniffing and changing position on the platform, in a visual stimulus independent manner. In addition, head and body angle changes result in pixel jitter, and therefore contour and head angle artifacts. These various sources of apparent head movements result in a wide range of head angular velocities in the same direction or opposite direction to the stimulus (Fig. 6a). Thus the head movements potentially triggered by the visual stimulus are embedded in a significant amount of unrelated head angle changes.

We reasoned that, in the absence of given visual cues, the random head movements would occur with relatively equal distributions in both clockwise and counterclockwise directions, and that visually driven responses, if occurring with enough frequency would bias this distribution in the stimulus (correct) direction. Given these considerations, we decided to compare globally the amount of head motions in the correct and incorrect directions. For this purpose we collected a data set of 10 animals (C57B/6) which we recorded under the reported optimal stimulus conditions (maximum contrast, spatial frequency 0.2 cyc/°, stimulus velocity 12°/s (Prusky et al., 2004; Umino et al., 2008; Kretschmer et al., 2013)) for 10 trials each. We then determined the number of frames containing head movements in the correct stimulus direction (nCorrect) or opposing direction (nWrong) with an angular head velocity window faster than V_{min} and slower than V_{max} . The amount of tracking was then computed as the ratio nCorrect/nWrong. In order to

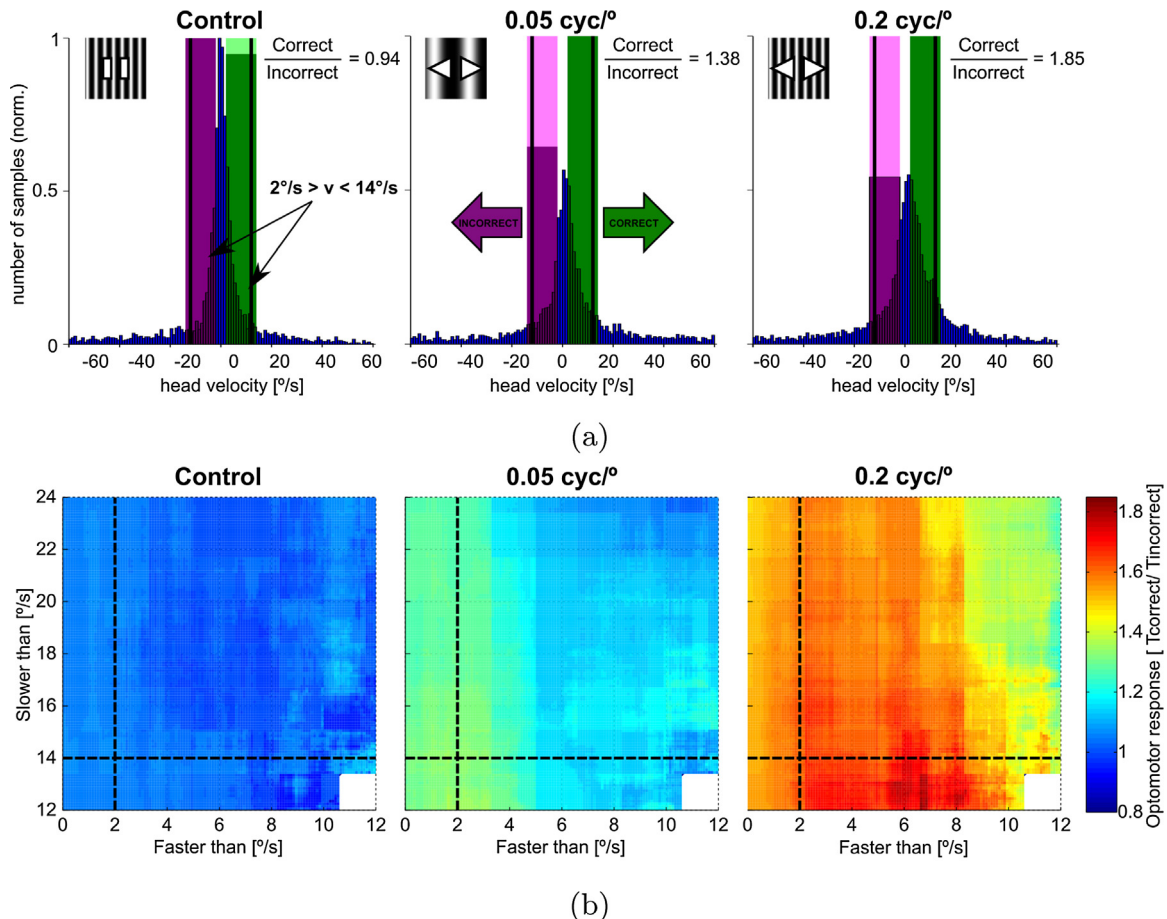


Fig. 6. Quantifying head movements during OMR experiments. (a) Illustration of OMR quantification. The histogram plots the number of frames for which the animal's head was moving with a given velocity in either stimulus direction ("correct", positive angle value) or against stimulus direction ("incorrect", negative value). Windows of head velocities of amplitudes and orientations similar to the stimulus velocity (correct, green), are compared to the windows of identical amplitudes but reversed orientation ("incorrect", magenta). The ratio between the sums in the correct and incorrect windows is defined as the Optomotor response. The histograms were calculated for all trials of one animal at the control condition (Left, 0.2 cyc/°, stimulus not moving), 0.05 cyc/° (Center) and 0.2 cyc/° (Right). (b) The effects of varying the thresholds for the windows defined in (a) on the determined value of the OMR. The x and y axes represent the slow and fast motion criteria, expressed in °/s. The heatmap color represents the amount of visually driven responses for each threshold criteria, expressed as number of tracking events in the correct vs. incorrect direction, illustrating the influence the thresholds have on the outcome of the analysis. The stippled lines determine the lower and upper bounds of the head velocity windows that were used for successive analysis. Data were collected from 10 animals, measured 10 times at each condition.

determine the window of velocities to be included in our analysis we systematically varied the upper and lower velocity thresholds V_{min} and V_{max} (V_{min} : 0°/s to 12°/s, V_{max} : 12°/s to 40°/s) and recorded the nCorrect/nWrong ratios for each condition (Fig. 6b). Low velocity thresholds ($V_{min} < 2°/s$) clearly reduced the ratio (Fig. 6b). The upper velocity threshold has less impact but a slight decrease of the ratio can still be observed at values of $V_{max} > 20°/s$. Under optimal stimulus conditions the tracking behavior and hence the nCorrect/nWrong ratio should be maximal, if the ideal threshold criteria were set. At the speed of 12°/s stimulus, chosen in our experiments, movements in a range of 2–14°/s seem to correlate well with stimulus direction.

Quantifying head movements. We can count the frames where the movement occurred in stimulus direction as:

$$T_{v_{head} \parallel v_{stim}} = f \in FRAMES : ||v_{stim}|| - 10°/s \leq ||v_{head}|| < ||v_{stim}|| + 2°/s \quad (11)$$

where $v_{head} \parallel v_{stim}$ (parallel velocities) and the movements against stimulus direction as:

$$T_{v_{head} \parallel -v_{stim}} = f \in FRAMES : ||v_{stim}|| - 10°/s \leq ||v_{head}|| < ||v_{stim}|| + 2°/s \quad (12)$$

where $v_{head} \parallel -v_{stim}$ (antiparallel velocities)

The ratio of the two sums is then used to quantify the response as:

$$OMR = \frac{T_{v_{head} \parallel v_{stim}}}{T_{v_{head} \parallel -v_{stim}}} \quad (13)$$

Fig. 6a illustrates the procedure. The boundaries are indicated by the cyan and green areas on the histogram for a stimulus running at 12°/s (blue line).

Further quality control. All recorded head and eye movement data were manually checked in a first step. For this purpose we developed two MATLAB tools to quickly browse through the traces of all recordings. In case of the head movements we implemented a program (BES) to browse through the recordings. The program allows us to discard segments in which the mouse was jumping from the platform consecutive times throughout an experiment. It also enables the user to retrack segments where the automated head tracking algorithm did not perform optimally due to a suboptimal setting of the threshold values (e.g. due to uneven or wet fur).

For this purpose the user can set a new color value and retrack the selected segment using the described tracking algorithm.

2.2.2. Eye movements

The eye tracker derives the x and y coordinates of the mouse eye (see Section 2.1.1). The recorded traces are the basis for an automatic detection of slow and fast components of the response. These data were used to quantify the Optokinetic reflex for each stimulus condition.

Detecting eye movements. We implemented the MATLAB program *eyeMovementMarker* to automatically detect and mark all slow and fast components within a recording. The detection is performed based on the following steps:

The trace (recorded at 120 Hz) is filtered with a moving average filter with a window of 10 samples. All continuous movements in stimulus direction with a minimum length of 20 samples are marked as slow components. If a movement in the opposite direction (minimal duration 10 samples) occurs directly after such a period, this event is considered to be the fast component of the OKR. The results are then displayed to the user, who can delete or merge periods manually. The pixel coordinates are converted into vertical and horizontal eye angles (azimuth and elevation) using the radius of pupil rotation (rp) previously derived through our calibration procedure (transformation described in Stahl, 2000).

Calibration of the system. The eye tracking system determines the x and y position of the pupil and one corneal reflection on the 512 px \times 256 px CCD sensor at 120 Hz. To derive the azimuth and elevation angles of the eye from this data, the system needs to be calibrated. Since the mouse cannot be asked or trained to orient its eye to a defined point in space the 3D center of the corneal curvature and the radius around which the pupil rotates are instead estimated from a series of images taken from defined angles by rotating the camera around the animal (Stahl et al., 2000). Instead of physically rotating the camera around the animal one can also translate the camera along an axis and then rotate it about its axis of rotation (Zoccolan et al., 2010). We adapted this methodology to our system. To avoid the camera being anywhere in the field of view of the animal we used a hot mirror (Edmund optics, NJ, USA Optics) to monitor the eye from above and performed such pseudo rotations by rotating the mirror instead of the camera. Fig. 7 shows this geometrical relationship. In order to determine the distance from the sensor of the camera to the mirror we performed a camera calibration procedure using a checkerboard pattern that was attached to the mirror. We used the Camera calibration toolbox for MATLAB (Bouguet, 2008). We followed all the calibration steps as described in Zoccolan et al. (2010) and implemented a MATLAB script that navigates the user through the procedure. Since our rails were not motorized the user had to translate the camera and mirror by hand and rotate the mirror. This was facilitated by the two electronic callipers that registered the position in real time. The circuitry from the callipers was connected to an Arduino Uno microcontroller board (Arduino LLC and Smart Projects S.R.L., Italy) through a custom circuitry to adjust their voltage for readout. The Arduino was connected to the Main PC through USB so that the location of the calipers was available from within the MATLAB script.

Validating the calibration procedure. We used a glass bead (radius 4 mm) to simulate a mouse eye. A circle was painted on the bead to represent the pupil. The pupil was rotated to a specific angle by using a 70 mm rotary stage (Edmund optics, NJ, USA). We performed two separate measurements to determine the precision and accuracy of the angle determination in the horizontal and vertical plane by mounting the rotary stage respectively. We performed the calibration procedure 5 times and determined the gaze angles at 20 different elevations and azimuth. The results are shown in Fig. 7a and b. In a range of 0–20° our calibration yields a mean error <1°.

The error is higher at large excursions ($\approx 2.5^\circ$ at -20° and $+20^\circ$). The precision (determined by calculating the mean standard deviation) was 0.43° for azimuth and 0.72° for elevation.

Quantifying eye movements. The total number, Gain, length, duration and amplitude of all movements are calculated for each individual trace based on the found onsets and offsets of the slow and fast components. The mean eye velocity to determine the gain is calculated using a linear regression over each detected time window.

2.2.3. Further analysis

All further steps in the analysis are automated, require no human interaction and are performed in the same way for head- and eye movements using our analysis framework *okranalyzer*.

During an experiment, the recording software automatically generates file names that contain all relevant stimulus parameters (e.g. spatial frequency, contrast, stimulus velocity, stimulus amplitude, mask used, etc.) for an experiment, complemented by a user defined prefix and suffix that typically indicates the ear tag of the animal and its age and/or genotype.

These parameters are parsed from the file names and allow us to automatize the analysis to some extent for any given condition. This meta data and data like the date and time of the experiment are stored in a structure that is maintained throughout all steps of analysis. A graphical user interface is provided to access this structure and easily select any subset of recordings and plot arbitrary dependency curves (e.g. median tracking performance of all 20 week old animals throughout all trials where the stimulus velocity was $12^\circ/\text{s}$ and the stimulus amplitude was 60 in relation to the spatial frequency). The provided tool chain can cover any upcoming experimental condition and is not limited to the current listed parameters.

2.3. Mouse handling, surgeries and experimental condition

C57BL/6 mice were kept in plexiglas cages ($46 \times 26 \times 16$ cm [$L \times W \times H$]) and housed at room temperature with a 12 h light/dark cycle. Food and water was available ad libitum. The mice were ear punched to recognize individuals. Experiments were conducted between 8 a.m. and 11 a.m. over a period of one week. We recorded Optomotor and Optokinetic responses of C57BL/6 mice using three different stimuli.

1. A control stimulus consisting of a sinusoidal grating with a spatial frequency of 0.2 cyc° which was not moving.
2. A stimulus with a low spatial frequency of 0.05 cyc° rotating at a velocity of $12^\circ/\text{s}$.
3. A stimulus with a spatial frequency of 0.2 cyc° (reported optimum) rotating at a velocity of $12^\circ/\text{s}$.

The moving stimuli alternated their direction every 5 s. We recorded 3 trials of 1 min for each condition. For the determination of the dual threshold criterion for the analysis of OMR experiments 5 male and 5 female animals were used. For the comparison of OKR and OMR we used 3 female and 2 male animals. All animals were 8–16 weeks old. All mouse handling procedures used in this study were approved by the National Eye Institute Animal Care and Use Committee (ACUC) under protocols NEI 640, NEI 651 and NEI 652. All NIH rodent surgery guidelines were followed.

2.3.1. Headpost surgery

All instruments were sterilized using a germ terminator dry glass bead sterilizer. A sterile environment was prepared and mice were anesthetized using an intraperitoneal Ketamine (80–120 mg/kg) and Xylazine (1–10 mg/kg) injection. Ophthalmic ointment was applied to the eyes to prevent corneal drying.

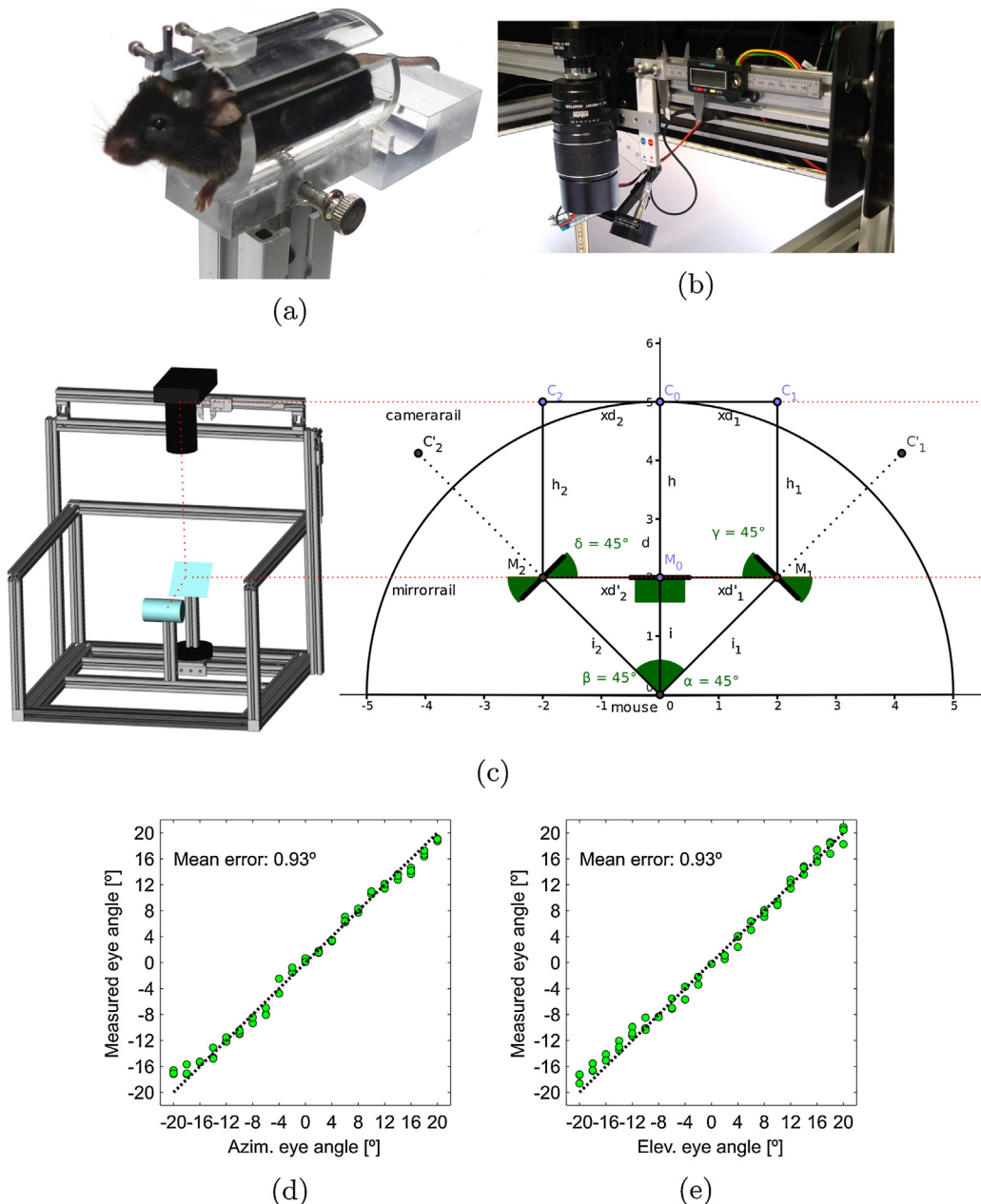


Fig. 7. (a) A mouse restrained in the acrylic holder. To derive the azimuth and elevation of the eye, the system needs to be calibrated. (b) Two callipers enable a precise translation of the camera. A laser pointer facilitates alignment of the camera and the hot mirror. (c) By translating the camera and rotating the mirror we can take multiple images of the eye from different virtual angles to calibrate the system. (d and e) Validation of the calibration procedure. Adjusted and measured angles across a range of 0–10° in the horizontal (d) and vertical (e) plane. The mean error was calculated as the mean difference between the actual angle and the measured angle.

Once the mouse was areflexic to paw pinch, the skin over the dorsal skull was opened with a 10 mm incision and the skull surface was washed with 3% hydrogen peroxide for about 30 s and then dried with a cotton swab. The skull was then washed several times with saline. Holes for four 1/16 in. diameter screws were drilled into the bone; the screws were inserted, and dental cement was used to fill the space between the screws. The metal head-post was then inserted into the mound to secure the animal during testing. More dental cement was used stabilize the head post. After the surgery that lasted \approx 15 m the mice were placed on a 37 °C heating pad. The mice typically awoke 40–60 m after surgery and were monitored for feeding, grooming, and gait. Buprenorphine (0.5 mg/kg) was delivered as needed for pain or discomfort. Eye movements were recorded not earlier than 48 h after surgery.

3. Results

3.1. Exemplary head and eye movements

In case of the measurement of head movements the animal is freely moving on the platform. The animal does not necessarily continuously participate in the experiment but instead may explore the platform or perform sniffing or grooming behavior. Fig. 8a shows three typical traces that were recorded at three different spatial frequencies. We quantify Optomotor responses as $OMR = (T_{v_{\text{head}} \parallel v_{\text{stim}}}) / (T_{v_{\text{head}} \parallel v_{\text{stim}}})$ (see Section 2.2.1). The total time the mouse was moving its head in the correct direction (stimulus direction) was more than 1.5× more than the time the mouse was moving in the incorrect direction at the reported optimal spatial frequency of 0.2 cyc/° (Kretschmer et al., 2013; Prusky et al., 2004).

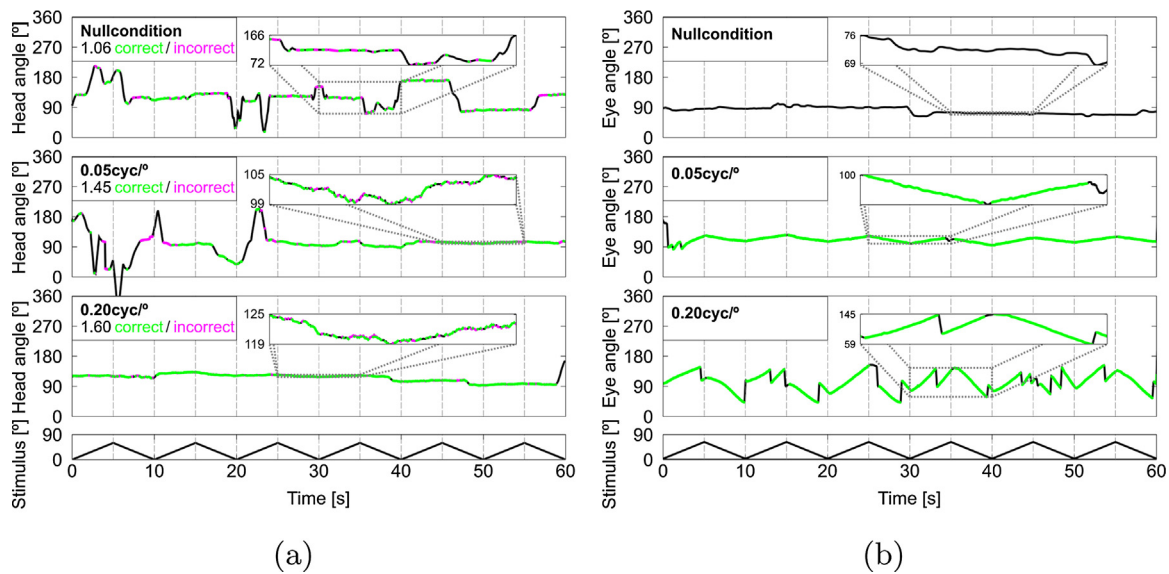


Fig. 8. Exemplary trace of recorded head (OMR) and eye movements (OKR) at three different stimulus conditions. The Nullcondition (0.2 cyc/s, stimulus not moving), and two spatial frequencies 0.05 cyc/s and 0.2 cyc/s presented with a stimulus rotating at 12°/s. Note the different scaling on the y-axes in the inserts.

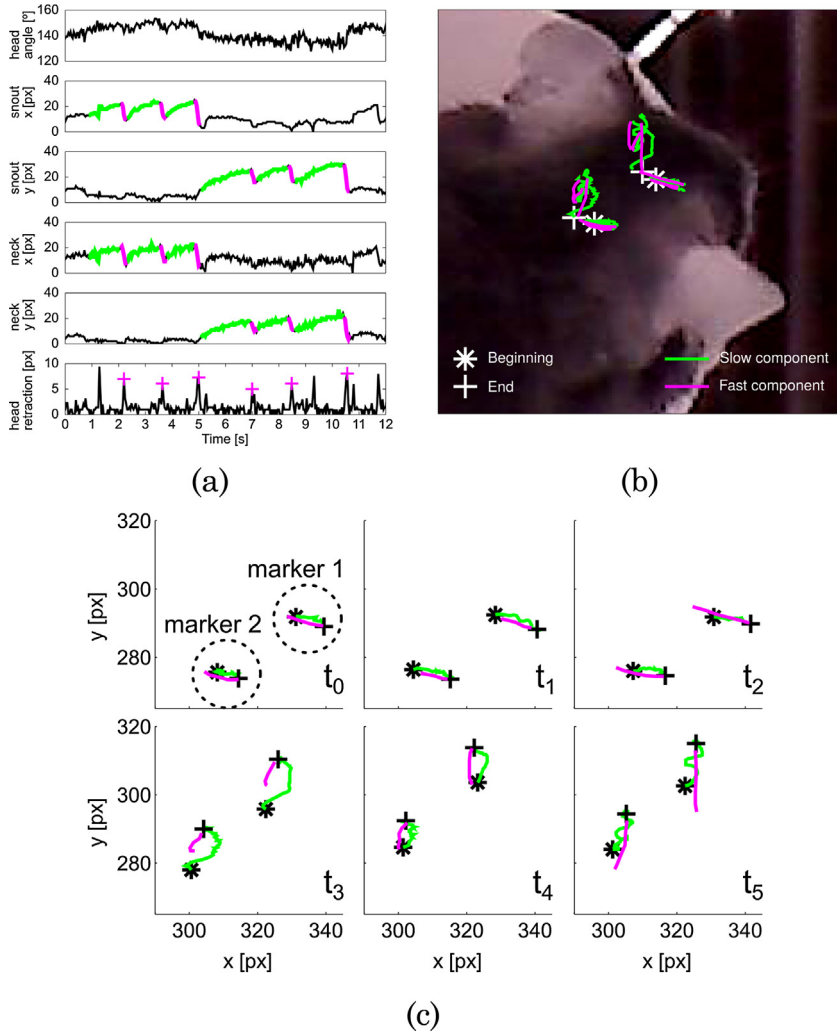


Fig. 9. The mouse head does not perform a homogeneous rotation. (a) The movement of the head is instead composed of a rotation and translation. To illustrate this phenomenon the x and y pixel coordinates of the two tracked locations of the forehead are plotted separately. (b) The animal performs head saccades that consist of a fast retraction of the head rather than a rotation opposite to stimulus direction as described in OKR. This retraction can be visualized by calculating the translation of the mouse head along the axis of gaze (bottom trace in (a)). (c) The time course of six individual slow phases (green), followed by fast phases (magenta). These periods occurred consecutively at time points t₀ to t₅. Traces are shown for both markers (Top: Marker 1, Bottom: Marker 2).

The ratio decreases at suboptimal values (see 0.05 cyc°) and is close to one when the stimulus is not turning (Nullcondition). The mouse hence moves its head as much in the correct as in the incorrect direction at Nullcondition. Fig. 10 shows the calculated Optomotor response at all stimulus conditions of all trials.

Optokinetic eye movements typically consist of two distinct components. A slow phase during which the eye moves in stimulus direction and a fast phase that follows the slow phase and occurs in the opposite direction (Cahill and Nathans, 2008). We occasionally observe a similar behavior based on the head movements. Fig. 9b shows the x and y coordinates of the two landmarks on the head (see Section 2.2.1). The isolated x and y translation of the head reveal distinct tracking periods that consist of slow periods in stimulus direction lasting up two 2 s and faster very short periods in the opposite direction. These fast periods can also be automatically detected as movements of the head along the axis between the two landmarks (Fig. 9a bottom trace). To our knowledge, this is the first report of head saccade movements during Optomotor recordings in mice. Surprisingly, the slow component of these head tracking movements consists of either pure translation (Fig. 9c, t0–t2) or combines rotation and translation (Fig. 9c, t3–t5).

Three exemplary traces of recorded eye movements are shown in Fig. 8b. The mouse is restrained and rarely performs spontaneous eye movements. Optokinetic responses occur during the entire minute. At low spatial frequencies (0.005 cyc°) the eye continuously follows the stimulus but does not perform resetting saccades (fast phase). At the optimal spatial frequency (0.2 cyc°) both the slow and the fast component of the response can be observed. We automatically detect the slow phases in the recordings.

Traditionally the gain (eye velocity/stimulus velocity) is used as a measure to determine the tuning of the visual system to the spatial and temporal aspects of the stimulus. Since we calibrated the system (see Section 2.2.2) we can calculate the velocity at which the eye followed and hence the gain (Azim. eye velocity/stimulus velocity). Fig. 10 illustrates the gain we measured in five animals.

4. Discussion

We present here a hardware apparatus and software suite designed to detect and analyze Optomotor and Optokinetic responses in mice. Our integrated stimulus display and data collection pipeline allows for the presentation of a large variety of stimuli coupled with the automated recording and analysis of head or eye movements, resulting in significantly improved OMR visual threshold determinations, and the first quantitative analysis of visually driven head movements in mice.

4.1. Stimulus presentation

Our setup can display visual stimuli on the inner surface of a freely rotating virtual sphere, ensuring that the mouse visual system perceives them under the same angle and at the same spatial resolution. A significant aspect of our stimulation conditions is that the visual stimulus can be centered in real time on the mouse head horizontal plane position, using feedback from our improved video tracking algorithm (see below). This feature is particularly useful when trying to assess the spatial resolution detected by the mouse, and facilitates the recording procedure, reducing the subjectivity of human participation in the experiment. The ability of masking allows us to cover portions of the visual field that correspond to defined areas like the binocular or monocular field of the animal. The ability to concomitantly translate and/or rotate the visual stimulus will allow the use of our setup in the design of other behavioral paradigms, including for instance looming behavior (Yilmaz and Meister, 2013).

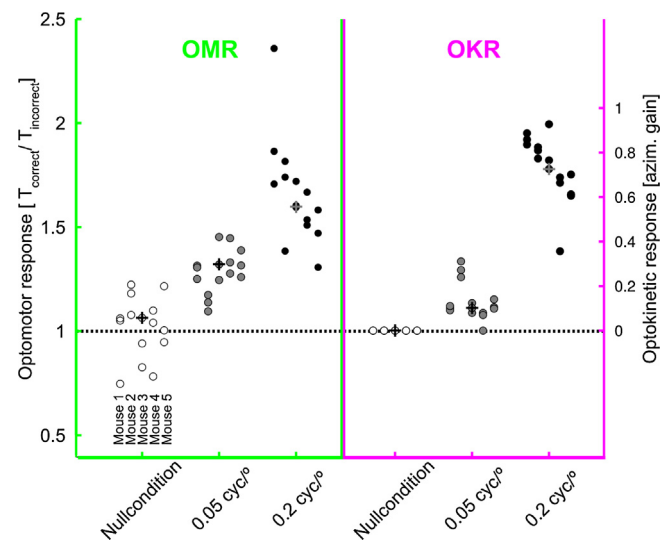


Fig. 10. Comparison of OKR and OMR in five C57BL/6 mice at three stimulus conditions. (i) Nullcondition, s stationary grating of 0.2 cyc° , (ii) a very low spatial frequency of 0.05 cyc° which is turning at $12^\circ/\text{s}$ and (iii) the reported optimal spatial frequency of 0.2 cyc° turning at $12^\circ/\text{s}$. OMR was quantified as described in Section 2.2.1. OKR is represented by the Gain (eye velocity/stimulus velocity). Three trials were measured for each animal. In both OMR and OKR experiments, the individual trials for each of five mice, are represented in separate columns at each stimulus condition. The exemplary trials depicted for mouse 3 in Fig. 8a and b are marked with a cross. Note that random head movements under Nullcondition result in an Optomotor response index centered around 1. No eye movements are detected under the Nullcondition (OKR Gain = 0). Both OMR and OKR increase at optimal spatial frequency (0.2 cyc°) compared to a lower special frequency (0.05 cyc°).

4.2. Quantifying OMR in mice

Our improved tracking algorithm (Section 2.1.1) can reliably identify animals of different coat color under photopic and scotopic light conditions. We determined the velocity range of stimulus correlated head movements (Fig. 6b) and found stimulus correlated head movements in a velocity range of $2\text{--}14^\circ/\text{s}$. This information is crucial to objectively quantify visually driven behavior in future. We introduce here a new global metric to quantify Optomotor responses in mice. We had previously found that the fraction of time at which stimulus correlated behavior occurs (Kretschmer et al., 2013) is not ideal in situations where an animal moves very little in general but still participates well in the experiment or when an animal is very agitated. By taking the ratio of all movements in the correct and incorrect directions we avoid this problem and can more directly compare the performance of different animals regardless of their overall activity status. Our tracking algorithm, enabling the determination of the actual trajectory of landmarks on the mouse head allows for a more precise description of the occurring Optomotor responses (Fig. 9a). We are now able to identify individual head retractions that follow a tracking period similarly to the fast component of the Optokinetic response. These movements do not seem to consist of a simple rotation of the head against stimulus direction but are more complex and seem to involve a strong translational component. For this type of head movements, one could derive the actual head gain of the slow component and use head saccades to quantify the response.

Compared to other methodologies our approach does not rely on human observation (Prusky et al., 2004) requiring trained personnel. Currently available setups require optimally several people performing the experiments to assure that the measurements are not biased by observer visual perception. The user is not only required to assess the animals visual performance but is also responsible for adjusting the position of the stimulus to keep the grating constant. While an automated readjustment has been

described before (Benkner et al., 2013; Kretschmer et al., 2013) our system allows us to directly measure spatio-temporal properties of the OMR, rather than relying on a binary decision criterion (Benkner et al., 2013; Prusky et al., 2004), under all stimulus conditions. Due to the lack of additional illumination and a limitations of the tracking algorithm the previously published approach (Kretschmer et al., 2013) was limited to photopic conditions.

A direct assessment of the reflex enables a measurement of parameters that would otherwise only be indirectly possible by varying a secondary parameter (e.g. contrast to measure contrast sensitivities at various spatial frequencies). This significantly speeds up experiments. This was previously possible (Kretschmer et al., 2013) but the improved tracking algorithm allowed us to apply a much more stringent criteria and enable a far more detailed analysis of OMR. We are for the first time able to directly validate and compare OMR and OKR which allows for a more detailed analysis of compensatory reflexes under the exact same conditions.

4.2.1. Calibration of the eye tracking system

Our calibration procedure combines the advantages of several previously published methodologies: In order to maintain a complete 360° surrounding stimulus, our camera is not placed anywhere in the field of view of the animal (Zoccolan et al., 2010; Stahl et al., 2000) but is instead located above the animal (similar to van Alphen et al., 2010). The image is recorded through an infra red reflective mirror to see the eye. To calibrate the system under this arrangement we used a semi-automated calibration procedure involving electronic callipers to give a precise control of the elevation and translation of the camera. By combining the translation of the camera with a rotation of the mirror we are able to determine the position of the pupil and corneal reflections from various virtual viewpoints. A previous approach simulated rotations around the animal, by rotating and translating the camera ((Zoccolan et al., 2010)) but this required the camera to be in the animals field of view. All rotations and translations of the camera and mirror in our setup could be automatized by the use of stepper motors (similar to Zoccolan et al., 2010). Since the Eye Tracker also determines the pupil diameter one could easily integrate the measurement of the pupillary reflex into the existing system.

4.2.2. Comparison of OMR and OKR

One of the advantages of our setup is the ability to derive quantitative measures of gain for both reflexes in response to the same set of stimuli. Thus, the OKR gain we measured for five animals varied from ≈0.7 to ≈0.9. Similar values have been described before (van Alphen et al., 2009) at comparable stimulus conditions. While the OKR Gain can directly be compared to absolute values from previous studies, this is not possible in case of OMR due to the different nature of analysis. Qualitatively the results match previous findings very well: Mice seem to perform OMR (Prusky et al., 2004; Kretschmer et al., 2013) and OKR (van Alphen et al., 2009; Tabata et al., 2010) best at a spatial frequency of ≈0.1–0.2 cyc°. Reduced responses have been reported at lower spatial frequencies like 0.05 cyc° for both OMR (Prusky et al., 2004; Kretschmer et al., 2013) and OKR (van Alphen et al., 2009; Tabata et al., 2010).

The OMR performance of the animal correlates well with the OKR performance. Animals that perform better than other animals under one condition also outperform their litter mates in the other condition (Fig. 10).

A more detailed parallel of the two reflexes will be described in a follow-up study.

4.3. Software design

Our integrated software suite, facilitates recording and analysis in several ways. All components are interfaced through a

GUI. The program design is modular, and hence individual components, such as the stimulus display (okrarena) and tracking algorithm (omrmonitor) could also be used in entirely different behavioral paradigms in mice or other species. Stimulus generation is straightforward and flexible, and the entire stimulus, recording and analysis workflow is highly integrated. The software could run simultaneously on several machines controlled from one central computer through TCP/IP could potentially enable high throughput measurements. The tracking algorithm okrarena is free software under GNU GPLv3 license, is compatible with all major operating systems (GNU/Linux, MAC, Windows) and can be downloaded at openetho.com. In addition, all software components are available on request from either of the corresponding authors (the level of documentation for individual components varies and the software is provided as is).

4.4. Implication and future plans

Whereas OMR measurements have mostly benefited the clinical research community, in particular with regard to the study of disease and therapy models, the OKR analysis in mice has been typically related to the study of neuronal circuits, specifically vestibulo-ocular integration. The measurement of OMR responses in the freely behaving mouse allows us to quickly and objectively assess its vision. Such measurements can be performed periodically over a long time period and the methodology is hence suitable for screening studies on a large number of animals involving genetic manipulations, drug treatments, aging or retinal degenerations. The improved objectivity and ease of use of our setup makes it particularly useful for these purposes. The ability to precisely describe the trajectory of mouse head movements, allows their quantification and evaluation of relevant parameters, such as amplitude and gain. This will allow us a direct comparison with eye movements elicited by visual stimulation during OKR in the same setup. This comparison will be interesting from the clinical investigation perspective, since it will better relate OMR data to the wealth of visual circuit knowledge available to the eye motion field. It will also be interesting to the visual circuit community, since it will allow for the direct comparison of OMR and OKR contribution to gaze stabilization. Given the flexibility of our setup, it will be interesting to explore other visually driven head and eye movements, and their perturbations in normal and pathologic conditions.

Acknowledgements

Hugh Cahill has provided guidance with implementing the head surgeries and designing the head fixation apparatus. Felix Ighovie Onojafe has provided technical help with head surgery optimization. Haohua Qiang has helped with calibration and measurement of screen light intensities under scotopic and photopic conditions. Lance Optican has provided helpful suggestions and critical reading of the manuscript. Funding for this work was provided by the Intramural Research Program of the National Eye Institute.

References

- Abdeljalil J, Hamid M, Abdel-Mouttalib O, Stéphane R, Raymond R, Johan A, et al. The optomotor response: a robust first-line visual screening method for mice. *Vision Res* 2005;45(11):1439–46. <http://dx.doi.org/10.1016/j.visres.2004.12.015>.
- Anstis S, Hutahajan P, Cavanagh P. Optomotor test for wavelength sensitivity in guppyfish (*Poecilia reticulata*). *Vision Res* 1998;38(1):45–53.
- Beck JC, Gilland E, Tank DW, Baker R. Quantifying the ontogeny of optokinetic and vestibuloocular behaviors in zebrafish, medaka, and goldfish. *J Neurophysiol* 2004;92(6):3546–61. <http://dx.doi.org/10.1152/jn.00311.2004>.
- Benkner B, Mutter M, Ecke G, Münch TA. Characterizing visual performance in mice: an objective and automated system based on the optokinetic reflex. *Behav Neurosci* 2013;127(5):788–96. <http://dx.doi.org/10.1037/a0033944>.

- Bouguet JY. Camera calibration toolbox for MATLAB. World Wide Web Electronic Publication; 2008] http://www.vision.caltech.edu/bouguetj/calib_doc/.
- Cahill H, Nathans J. The optokinetic reflex as a tool for quantitative analyses of nervous system function in mice: application to genetic and drug-induced variation. *PLoS ONE* 2008];3(4):e2055, <http://dx.doi.org/10.1371/journal.pone.0002055>.
- Dräger UC. Observations on monocular deprivation in mice. *J Neurophysiol* 1978];41(1):28–42.
- Dubois MF, Collewijn H. Optokinetic reactions in man elicited by localized retinal motion stimuli. *Vision Res* 1979];19(10):1105–15.
- Easter S Jr, Nicola GN. The development of vision in the zebrafish (*Danio rerio*). *Dev Biol* 1996];180(2):646–63.
- Iwashita M, Kanai R, Funabiki K, Matsuda K, Hirano T. Dynamic properties, interactions and adaptive modifications of vestibulo-ocular reflex and optokinetic response in mice. *Neurosci Res* 2001];39(3):299–311.
- Kretschmer F, Ahlers MT, Ammermüller J, Kretzberg J. Automated measurement of spectral sensitivity of motion vision during optokinetic behavior. *Neurocomputing* 2012];84:39–46.
- Kretschmer F, Kretschmer V, Kunze VP, Kretzberg J. Omr-area: automated measurement and stimulation system to determine mouse visual thresholds based on optomotor responses. *PLoS One* 2013];8(11):e78058, <http://dx.doi.org/10.1371/journal.pone.0078058>.
- Kretschmer F. Automatisiertes tracking von kopf- und augenbewegungen bei 360°-stimulation zur charakterisierung des visuellen systems kleiner wirbeltiere [Ph.D. thesis]. Fakultät für Informatik, Wirtschafts- und Rechtswissenschaften der Carl von Ossietzky Universität Oldenburg; 2012.
- Mangini NJ, Venable JW, Williams MA, Pinto LH. The optokinetic nystagmus and ocular pigmentation of hypopigmented mouse mutants. *J Comp Neurol* 1985];241(2):191–209, <http://dx.doi.org/10.1002/cne.902410207>.
- Mitchiner JC, Pinto LH, Venable JW. Visually evoked eye movements in the mouse (*Mus musculus*). *Vision Res* 1976];16(10):1169–71.
- Prusky GT, Alam NM, Beekman S, Douglas RM. Rapid quantification of adult and developing mouse spatial vision using a virtual optomotor system. *Invest Ophthalmol Vis Sci* 2004];45(12):4611–6, <http://dx.doi.org/10.1167/iovs.04-0541>.
- Rinner O, Rick JM, Neuhauss SCF. Contrast sensitivity, spatial and temporal tuning of the larval zebrafish optokinetic response. *Invest Ophthalmol Vis Sci* 2005];46(1):137–42, <http://dx.doi.org/10.1167/iovs.04-0682>.
- Sakatani T, Isa T. Pc-based high-speed video-oculography for measuring rapid eye movements in mice. *Neurosci Res* 2004];49(1):123–31, <http://dx.doi.org/10.1016/j.neures.2004.02.002>.
- Schmucker C, Seeliger M, Humphries P, Biel M, Schaeffel F. Grating acuity at different luminances in wild-type mice and in mice lacking rod or cone function. *Invest Ophthalmol Vis Sci* 2005];46(1):398–407, <http://dx.doi.org/10.1167/iovs.04-0959>.
- Sinex DG, Burdette LJ, Pearlman AL. A psychophysical investigation of spatial vision in the normal and reeler mutant mouse. *Vision Res* 1979];19(8):853–7.
- Stahl JS, van Alphen AM, Zeeuw CID. A comparison of video and magnetic search coil recordings of mouse eye movements. *J Neurosci Methods* 2000];99(1–2):101–10.
- Suzuki S, Abe K. Topological structural analysis of digitized binary images by border following. *Comput Vis Graph Image Process* 1985];30(1):32–46.
- Tabata H, Shimizu N, Wada Y, Miura K, Kawano K. Initiation of the optokinetic response (OKR) in mice. *J Vis* 2010];10(1), <http://dx.doi.org/10.1167/10.1.13>.
- Tappeiner C, Gerber S, Enzmann V, Balmer J, Jazwinska A, Tschopp M. Visual acuity and contrast sensitivity of adult zebrafish. *Front Zool* 2012];9(1):10, <http://dx.doi.org/10.1186/1742-9994-9-10>.
- Thaung C, Arnold K, Jackson IJ, Coffey PJ. Presence of visual head tracking differentiates normal sighted from retinal degenerate mice. *Neurosci Lett* 2002];325(1):21–4.
- Umino Y, Solessio E, Barlow RB. Speed, spatial, and temporal tuning of rod and cone vision in mouse. *J Neurosci* 2008];28(1):189–98, <http://dx.doi.org/10.1523/JNEUROSCI.3551-07.2008>.
- van Alphen B, Winkelmann BHJ, Frens MA. Age- and sex-related differences in contrast sensitivity in C57BL/6 mice. *Invest Ophthalmol Vis Sci* 2009];50(5):2451–8, <http://dx.doi.org/10.1167/iovs.08-2594>.
- van Alphen B, Winkelmann BHJ, Frens MA. Three-dimensional optokinetic eye movements in the C57BL/6 mouse. *Invest Ophthalmol Vis Sci* 2010];51(1):623–30, <http://dx.doi.org/10.1167/iovs.09-4072>.
- Yilmaz M, Meister M. Rapid innate defensive responses of mice to looming visual stimuli. *Curr Biol* 2013];23(20):2011–5, <http://dx.doi.org/10.1016/j.cub.2013.08.015>.
- Zoccolan D, Graham BJ, Cox DD. A self-calibrating, camera-based eye tracker for the recording of rodent eye movements. *Front Neurosci* 2010];4:193, <http://dx.doi.org/10.3389/fnins.2010.00193>.